DSPACE

https://dspace.org/

The attenuation of the main zone at the Phosiri Dome, Bushveld Complex

Martin, Lucienne E

2011-05-16
http://hdl.handle.net/10539/9776

Downloaded from a DSpace repository. https://dspace.org/

The copyright of the above-mentioned described thesis rests with the author or the University to which it was submitted. No portion of the text derived from it may be published without the prior written consent of the author or University (as may be appropriate). *Short quotations may be included in the text of a thesis* or dissertation for purposes of illustration, comment or criticism, provided full acknowledgement is made of the source, author and University.

The Attenuation of the Main Zone at the Phosiri Dome, Bushveld Complex

Lucienne E. Martin

Dissertation submitted in fulfilment of the
requirements for the degree of

Master of Science

in the Department of Geology,
University of the Witwatersrand,
Johannesburg.

Supervisor: Professor R. G. Cawthorn

March, 1999

Declaration

All work contained within this thesis is the original work of the author, except where specific references acknowledge the work of others. It is being submitted for the degree of Master of Science at the University of the Witwatersrand, Johannesburg. It has not been submitted before, for any degrees or examination in any other university.

Signed



Lucienne E. Martin 17/3/99

ABSTRACT

The Phosiri Dome, located in the eastern limb of the Bushveld Complex in South Africa, is a structurally uplifted area containing the ultramafic-mafic rocks of the Rustenburg Layered Suite. Two cores taken from boreholes drilled into the southern flank of the dome, during exploration of the region between 1990 and 1997, were analysed using petrographic, geochemical and isotopic methods. The aim of the analysis was to gain a comprehensive understanding of the geology, such that it could be compared to the typical sequence of the Rustenburg Layered Suite, and any anomalies or unexpected phenomena identified. It was anticipated that the analysis would contribute to an understanding of the mechanisms at work in similarly attenuated lithologies. In addition, the work would provide data to support future exploration activities for extracting mineral resources.

The analysis revealed that, although much of the zonal structure of the Rustenburg Layered Suite was present in the deeper of the two boreholes, at 772m thick, the sequence was severely attenuated from the more typically expected 8km thickness. The attenuation included both the thinning of individual layers and the complete absence of others, including the single largest sequence: Subzone B of the Main Zone. Significantly, the complete Merensky Reef is present at a depth of only 480m.

A number of models can be postulated to explain the absence of the lithologies, and include non-deposition, thinning and faulting processes. There are possible periods of non-deposition and thinning occurring in the lower reaches of the sequence, with late stage faulting affecting the entire sequence. Subsequent hydrothermal alteration of the lithologies either side of these fault zones, throughout the majority of the sequence, is present at Phosiri.

CONTENTS

1: PURPOSE OF STUDY p1

1.1: Background p1
1.2: Study Aim and Objectives p1
1.3: Synopsis of Study Techniques p1

2: GEOLOGICAL SETTING OF THE BUSHVELD COMPLEX p3

2.1: Introduction p3
2.2: Floor Rocks and their Relationship to the Rustenburg Layered Suite p5
2.3: Roof Rocks and Relationship to the Bushveld Complex p6
2.4: Mineral Assemblage of the Rustenburg Layered Suite p7
2.5: Stratigraphic Classification p7
2.5.1: Marginal Zone p8
2.5.2: Lower Zone p9
2.5.3: Critical Zone p9
2.5.4: Main Zone p11
2.5.5: Upper Zone p13
2.6: Magmatic Influxes p14
2.7: Connectivity of the Eastern and Western Limbs p14

3: THE STUDY AREA p16

3.1: Location p16
3.2: Geology of the Phosiri Dome p16
3.3: Previous Investigations p17
3.4: Location of Boreholes D1 and D2 p18

4: BOREHOLE LOG DESCRIPTIONS p19

4.1: Borehole D1 p19
4.2: Borehole D2 p23

5: PETROGRAPHIC OBSERVATIONS p26

5.1: D1 Petrographic Descriptions p26
5.2: D2 Petrographic Descriptions p32
5.3: Comparisons of Borehole Observations and Petrographic Analyses with the Typical Sequence for the Eastern Bushveld Complex p36

6: MINERAL ANALYSES p42

6.1: Electron Microprobe Analysis p42
6.1.1: Borehole D1 p43
6.1.1.1: Clinopyroxene p43
6.1.1.2: Orthopyroxene p44
6.1.1.3: Plagioclase p45
6.1.1.4: D1 Summary p47
6.1.1.5: Wo-En-Fs Ternary Systems p48
6.1.2: Borehole D2 p57
6.1.2.1: Clinopyroxene p57
6.1.2.2: Orthopyroxene p58
6.1.2.3: Plagioclase p59
6.1.2.4: D2 Summary p60
6.1.2.5: Wo-En-Fs Ternary Systems p60
6.2: Magnetite Separates p67
6.2.1: Borehole D2 p67
6.2.2: Comparisons with Magnetite Layers of the Eastern Limb with Samples Taken from the Phosiri Dome p69
6.3: Comparison of Mineral Analyses and the Typical Sequence of the Eastern Bushveld Complex p71

7: WHOLE ROCK XRF GEOCHEMISTRY p75

7.1: Borehole D1 p75
7.2: Summary of D1 p79
7.3: Borehole D2 p82
7.4: Summary of D2 p85
7.5: Element Correlations for D1 and D2 Boreholes with Typical Values from the Bushveld Complex p89
7.6: Comparison of Whole Rock XRF Geochemistry Analysis with Typical Data for the Eastern Bushveld Complex p93

8: STRONTIUM ISOTOPE ANALYSIS p96

8.1: Borehole D1 p97
8.1.1: Sr (ppm) p97
8.1.2: Rb (ppm) p97
8.1.3: R_O at 2060Ma p98
8.1.4: Summary of D1 p98
8.2: Borehole D2 p101
8.2.1: Sr (ppm) p101
8.2.2: Rb (ppm) p101
8.2.3: R_O at 2060Ma p101
8.2.4: Summary of D2 p101
8.3: Comparisons of Strontium Isotope Analyses and the Typical Sequence of the Bushveld Complex. p103

9: DISCUSSION AND CONCLUSIONS p106

9.1: Models for the Attenuation of the Phosiri Dome p106
9.1.1: Lateral Variation in the Extent of Magmatic Influx. p106
9.1.2: Thinning of the Mafic Sequence Units in the Vicinity of the Diapiric Structure p107
9.1.3: Faulting Out of Mafic Units p107
9.1.4: Magmatic Influxes Subjected to Different Magma Mixing and Differentiation Processes p107

9.2: Critical Zone p107
9.3: Main Zone p109
9.4: Upper Zone p109
9.5: Overview p110
9.6: Further Work p111

APPENDICES

APPENDIX 1: Borehole Log Descriptions i - vi
APPENDIX 2: Petrographic Descriptions vii - xxiii
APPENDIX 3: Electron Microprobe Standards xxiv - xxv
APPENDIX 4: Electron Microprobe Data xxvi - lxii
APPENDIX 5: XRF standards lxiii
APPENDIX 6: XRF whole rock Geochemical Data lxiv - lxxi

ACKNOWLEDGEMENTS

BIBLIOGRAPHY

LIST OF FIGURES

Figure 2.A The Bushveld Complex with the eastern limb outlined. p4

Figure 2.B The eastern limb of the Bushveld Complex (after Sharpe and Chadwick, 1982 and Lea, 1996). The southern portion of the Phosiri Dome is outlined. p6

Figure 2.C Simplified stratigraphic log of the Bushveld Complex, with appropriate thicknesses of zones and subzones indicated to the left of the columns in meters, as found in the eastern limb. (After Eales and Cawthorn, 1996, with data from the eastern limb compiled from Von Gruenewaldt, 1973, Molyneux, 1974 and Cameron, 1978). p8

Figure 3.A The Phosiri Dome, bounded in the west by the Wonderkop Fault (after Sharpe and Chadwick, 1982), with the locations of boreholes D1 and D2 indicated. p17

Figure 3.B Schematic cross section showing the relationship between boreholes D1 and D2 and the Bushveld Complex units. p18

Figure 4.A Stratigraphic log of borehole D1. p22

Figure 4.B Stratigraphic log of borehole D2. p25

Figure 5.A Deformation of plagioclase pericline twinning. p30

Figure 5.B Deformation of twinning in plagioclase. p30

Figure 5.C Ductile deformation of orthopyroxene with augite exsolution lamellae. p30

Figure 5.D Deformation of pyroxene resulting in a wavy appearance. p30

Figure 5.E Magnetite enclosing pyroxene and in filling fractures within the pyroxenes. p30

Figure 5.F Needles of biotite extending from the pyroxene and cutting across the plagioclase. p30

Figure 5.G As for Figure 5.A but with chlorite alteration of the pyroxene. p31

Figure 5.H Extensive epidotisation of grains within a mixed gabbro-norite-pyroxenite assemblage. p31

Figure 5.I Extensive alteration to clays, epidote and chlorite within a spotted anorthosite. p31

Figure 5.J Primary hornblende with quartz and plagioclase. p31

Figure 5.K Secondary hornblende with remnant ophitic textures between plagioclase and the original pyroxene. p31

Figure 5.L Plagioclase encapsulated within orthopyroxene. p35

Figure 5.M Rounded grains of plagioclase exhibiting myrmekitic texture. p35

Figure 5.N Pericline and albite twinning. p35

Figure 5.O Inverted pigeonite with plagioclase enclosed, exhibiting an ophitic texture. p35

Figure 5.P Sub-parallel alignment of magnetite exsolution needles in orthopyroxene. p35

Figure 5.Q Borehole sections from Atok, Messina and D1 borehole, located between the footwall to the Merensky Reef to the hangingwall to the Bastard Reef. p38

Figure 5.R The Main Zone sequence as found in the D1 and D2 boreholes, compared with the typical sequence of the eastern Bushveld Complex. p41

Figure 6.A Electron microprobe analyses of clinopyroxene cores and rims from samples in D1. The Mg content, wt % TiO_2, Al_2O_3 and Cr_2O_3 are plotted against the stratigraphic column and depth relative to the MZ/UZ boundary, which includes the positions of the Merensky Reef (MR) and Bastard Reef (BR). p48

Figure 6.B Electron microprobe analyses of orthopyroxene cores and rims from samples in D1. The En content, wt % TiO_2, Al_2O_3 and Cr_2O_3 are plotted against the stratigraphic column and depth relative to the MZ/UZ boundary, which includes the positions of the Merensky Reef (MR) and Bastard Reef (BR). p49

Figure 6.C Electron microprobe analyses of plagioclase cores and rims from samples in D1. The An content, wt % K_2O and FeO are plotted against the stratigraphic column and depth relative to the MZ/UZ boundary, which includes the positions of the Merensky Reef (MR) and Bastard Reef (BR). p50

Figure 6.D D1 clinopyroxene and orthopyroxene pairs plotted with isotherms calculated for 0 Kbar, after Davidson and Lindsley (1989). p51

Figure 6.E Electron microprobe analyses of clinopyroxene cores and rims from D2. The Mg content, wt % TiO_2, Al_2O_3 and Cr_2O_3 are plotted against the stratigraphic log and depth relative to the MZ/UZ boundary. p61

Figure 6.F Electron microprobe analyses of orthopyroxene cores and rims from D2. The En content, wt % TiO_2, Al_2O_3 and Cr_2O_3 are plotted against the stratigraphic log and depth relative to the MZ/UZ boundary. p61

Figure 6.G Electron microprobe analyses of plagioclase cores and rims from D2. The An content, wt % K_2O and FeO are plotted against the stratigraphic log and depth relative to the MZ/UZ boundary. p62

Figure 6.H D2 clinopyroxene and orthopyroxene pairs plotted with isotherms calculated for 0Kbar, after Davidson and Lindsley (1989). p63

Figure 6.I XRF analyses of magnetite separates from D2. The wt % TiO_2, V_2O_5 and Cr ppm are plotted against the stratigraphic column and depth relative to the MZ/UZ. Magnetite layers are represented as horizontal dashed lines. p68

Figure 6.J TiO_2 - V_2O_5 - Cr_2O_3 ternary plot of magnetites within D2 and on surface, with solid blue symbols representing the magnetite layers within D2. The subzones here are A, B and C, as referred to by Klemm *et al.* (1985). p70

Figure 6.K Comparative data for the eastern and western Bushveld Complex. Dimensions of the shaded areas are defined by the maximum and minimum values from the core analyses of cumulus pyroxenes and plagioclase determined in D1 and D2. Thicknesses of each shaded area are delimited by the points of intersection with the data of Von Gruenewaldt (1973), Molyneux (1974) and Mitchell (1986). The positions of the Merensky Reef (MR) and Pyroxenite Marker (BR) are indicated. p73

Figure 6.N Comparative data, as for Figure 6.K, with Subzone B of the Main Zone removed so that Subzone C directly overlies Subzone A. P74

Figure 7.A XRF analyses of whole rock samples from D1. The Mg #, wt % TiO_2 and Al_2O_3 are plotted against the stratigraphic column and depth relative to the MZ/UZ boundary, which includes the positions of the Merensky Reef (MR) and Bastard Reef (BR). P80

Figure 7.B XRF analyses of whole rock samples from D1. The Sr and Zr ppm contents and wt % K_2O are plotted against the stratigraphic column and depth relative to the MZ/UZ boundary, which includes the positions of the Merensky Reef (MR) and Bastard Reef (BR). P80

Figure 7.C XRF analyses of whole rock samples from D1. The interelement ratios Cr/Co, Co/V, Cr/V and Sr/Al_2O are plotted against the stratigraphic column and depth relative to the MZ/UZ boundary, which includes the positions of the Merensky Reef (MR) and Bastard Reef (BR). All elements are measured as ppm, except for wt % Al_2O_3. P81

Figure 7.D XRF analyses of whole rock samples from D2. The Mg #, wt % TiO_2 and Al_2O_3 are plotted against the stratigraphic column and depth relative to the MZ/UZ boundary. p87

Figure 7.E XRF analyses of whole rock samples from D2. The Sr and Zr ppm contents and wt % K_2O are plotted against the stratigraphic column and depth relative to the MZ/UZ boundary. p87

Figure 7.F XRF analyses of whole rock samples from D2. The interelement ratios Cr/Co, Co/V, Cr/V and Sr/Al_2O are plotted against the stratigraphic column and depth relative to the MZ/UZ boundary. All elements are measured as ppm, except for wt % Al_2O_3. p88

Figure 7.G XRF element correlations. (A) wt % Al_2O_3 v CaO for D1, (B) wt % Al_2O_3 v CaO for D2, (C) wt % MgO v Sr ppm for D1, with data from Cawthorn (1996) for directly above and below the Merensky Reef (MR), and (D) wt % MgO v Sr ppm for D2. The blue stars in (A) and (C) depict data from the Merensky and Bastard Reef interval. p91

Figure 7.H XRF element correlations. (A) wt % Al_2O_3 v Sr ppm for D1, (B) wt % Al_2O_3 v Sr ppm for D2, (C) wt % Al_2O_3 v MgO for D1, with data from Cawthorn (1996) and (D) wt % Al_2O_3 v MgO for D2. The blue stars in (C) depict data from the Merensky and Bastard Reef interval. p92

Figure 7.I XRF element correlations. (A) wt % MgO v Cr ppm for D1, (B) wt % MgO v Cr ppm for D2, (C) Ni ppm v V ppm for D1, and (D) Ni ppm v V ppm for D2. p92

Figure 7.J Comparative XRF data from Mitchell (1986) in the western limb of the Bushveld Complex. p95

Figure 8.A Strontium isotope initial ratios (R_O at 2060Ma) and the Sr ppm content for samples from D2, plotted against the stratigraphic column and depth relative to the MZ/UZ boundary, which includes the positions of the Merensky Reef (MR) and Bastard Reef (BR). p100

Figure 8.B Strontium isotope initial ratios (R_O at 2060Ma) and the Sr ppm content of samples from D2, plotted against the stratigraphic column and depth relative to the MZ/UZ boundary, which includes the positions of the Merensky Reef (MR) and Bastard Reef (BR). p102

Figure 8.C Complete initial profile of the initial ratio through the Bushveld Complex in the western limb, after Kruger (1994), with data acquired from Teigler (1990), Eales *et al.* (1990), Mitchell (1986), Cawthorn *et al.* (1991) and Kruger *et al.* (1987). p105

Figure 9.A Schematic representation of the cross section of the Bushveld Complex Units between D1 and D2. The boundaries between Subzones A, B and C of the Main Zone are inferred to pinch out towards the Phosiri Dome in the northeast. p111

LIST OF TABLES

Table 5.i Summary of petrographic observations from D1 thin sections. p29

Table 5.ii. Summary of D2 thin section observations. p34

Table 6.i Standard deviations as calculated from data run on three standards, with a total of 90 points being measured (30 points on each standard). p42

Table 6.ii Average D1 clinopyroxene values for both core and rim analyses as determined by electron microprobe, with Fe^{3+} calculated from stoichiometry. p52

Table 6.iii Average D1 orthopyroxene values for both core and rim analyses as determined by electron microprobe, with Fe^{3+} calculated from stoichiometry. p53

Table 6.iv Average D1 plagioclase core and rim analyses as determined by electron microprobe. p54

Table 6.v Plagioclase separates data as determined by XRF on fusion discs. p55

Table 6.vi Electron microprobe analyses for average clinopyroxene cores and rims for borehole D2, with Fe^{3+} calculated from stoichiometry. p64

Table 6.vii D2 orthopyroxene average core and rim analyses as determined by electron microprobe, with Fe^{3+} calculated from stoichiometry. p65

Table 6.viii Average plagioclase core and rim analyses for borehole D2, determined by electron microprobe. p66

Table 6.ix D2 Borehole magnetite layers samples, where depth (m) is relative to the MZ/UZ boundary. p68

Table 6.x Ground surface samples taken from the flanks of the Phosiri Dome. p68

Table 7.i Representative data from both D1 and D2 showing the XRF values for the particular units as described. p86

Table 8.i Strontium Isotopic analyses for borehole D1, as determined by Mass Spectrometry. Shaded areas indicate samples that were selected to test the effects of alteration, with duplication of D1.316 to ensure reproducibility. p99

Table 8.ii Strontium Isotopic analyses for borehole D2, as determined by Mass Spectrometry. p102

1: PURPOSE OF STUDY

1.1: Background

The main mineable sources of platinum and Platinum Group Elements (PGE's) in the Bushveld Complex of South Africa, are in areas where the Merensky Reef is found either as an outcrop, or at a shallow depth. As resources became increasingly depleted, structurally uplifted areas that had previously been ignored came under investigation. The Phosiri Dome, also known as the Fortdraai Anticline, is one such uplifted area, although the structure and the processes involved in its creation are not well understood. Confirmation from drilling programmes that mineable horizons were, indeed, close to the surface, created an opportunity to examine the dome's structure in greater detail and, potentially, to improve the understanding of how mafic units form in such circumstances.

Two borecores, taken from the southern flank of the Dome, were made available to the University of the Witwatersrand for detailed analysis.

1.2: Study Aim and Objectives

The aim of this study was to undertake a comprehensive geological analysis of two existing borehole cores taken from the southern flank of the Phosiri Dome. Within this aim, the study sought to meet the following objectives:

- To construct a typical stratigraphic sequence for the Bushveld Complex from an extensive literature search of the existing data.
- To determine the relationship between the borecore data and the typical sequence expected for the Bushveld Complex.
- To identify any unexpected phenomena.
- To provide data to support the understanding of attenuated lithologies at similar locations.
- To provide data to support future exploration activities for identifying mineral resources.

1.3: Synopsis of Study Techniques

The data analysed in this study were derived from material collected from the two boreholes. Samples extracted from the drillcore sections were divided for thin section preparation, prior to petrographical examination, and for geochemical and isotopic analyses. The following equipment and techniques were employed:

- Petrographic Microscope. A Leitz Wetzlar, type 307-148.001 (Mag. x 100 - 400), was used for thin section analysis.
- Digital Camera. A Leica DC 100 was used to photograph particular features found within individual grains of the minerals observed under the microscope.
- Electron microprobe. The electron microprobe was used to analyse the chemical composition of individual clinopyroxene, orthopyroxene and plagioclase grains.
- X-Ray Florescence (XRF). XRF was used to analyse: whole rock samples, prepared as powder briquettes and fusion discs; magnetite samples from D2 and ground level, prepared as briquettes; and plagioclase separates, prepared as fusion discs.
- Mass Spectrometry. Plagioclase separates were also used to determine the strontium isotope initial ratio of the lithological units within the boreholes, using Mass Spectrometry.

2: GEOLOGICAL SETTING OF THE BUSHVELD COMPLEX

2.1: Introduction

The following descriptions are of rocks, minerals, zones, subzones and magmatic fluxes pertaining to the eastern limb of the Bushveld Complex, except where stated.

The Bushveld Complex comprises three main suites of igneous rocks: the Rooiberg Group Volcanics; the Rustenburg Layered Suite (RLS), which is the main plutonic phase of the ultramafic-mafic layered rocks; and the Bushveld Granites, which represent the final event.

The Complex is 2060 ± 27 Ma years old (Walraven *et al.*, 1990) and situated within the Transvaal Supergroup basin. A predominantly granitic block of Archaean craton forms the basement of the basin, which Sharpe *et al.* (1981) believed had originally extended over a greater area than the 290 x 550km surface outcrop evident today. Figure 2.A shows the RLS in relation to both the Transvaal Supergroup and the Archaean basement. The RLS extends from north of Villa Nora to south of Stoffberg and from west of Neitverdiend to Burgersfort in the east. The ultramafic-mafic layered rocks intruded into the Transvaal Supergroup at the level of the Upper Pretoria Group, generally along bedding planes (Coertze, 1970). The alternating cyclic package of sediments and volcanics of the Pretoria Group and Rooiberg Group Volcanics have been dated to be between 2300 and 2200 Ma years old (Button, 1976). A more recent date acquired by Walraven *et al.* (1990) puts the Rooiberg Volcanics at 2060Ma. Cheney and Twist (1991) maintained that the sediments have either been removed or uplifted. Button (1976) pointed out that the amount removed varies from location to location across the entire complex and he estimates that, in the eastern limb, a thickness of 4700m has been replaced.

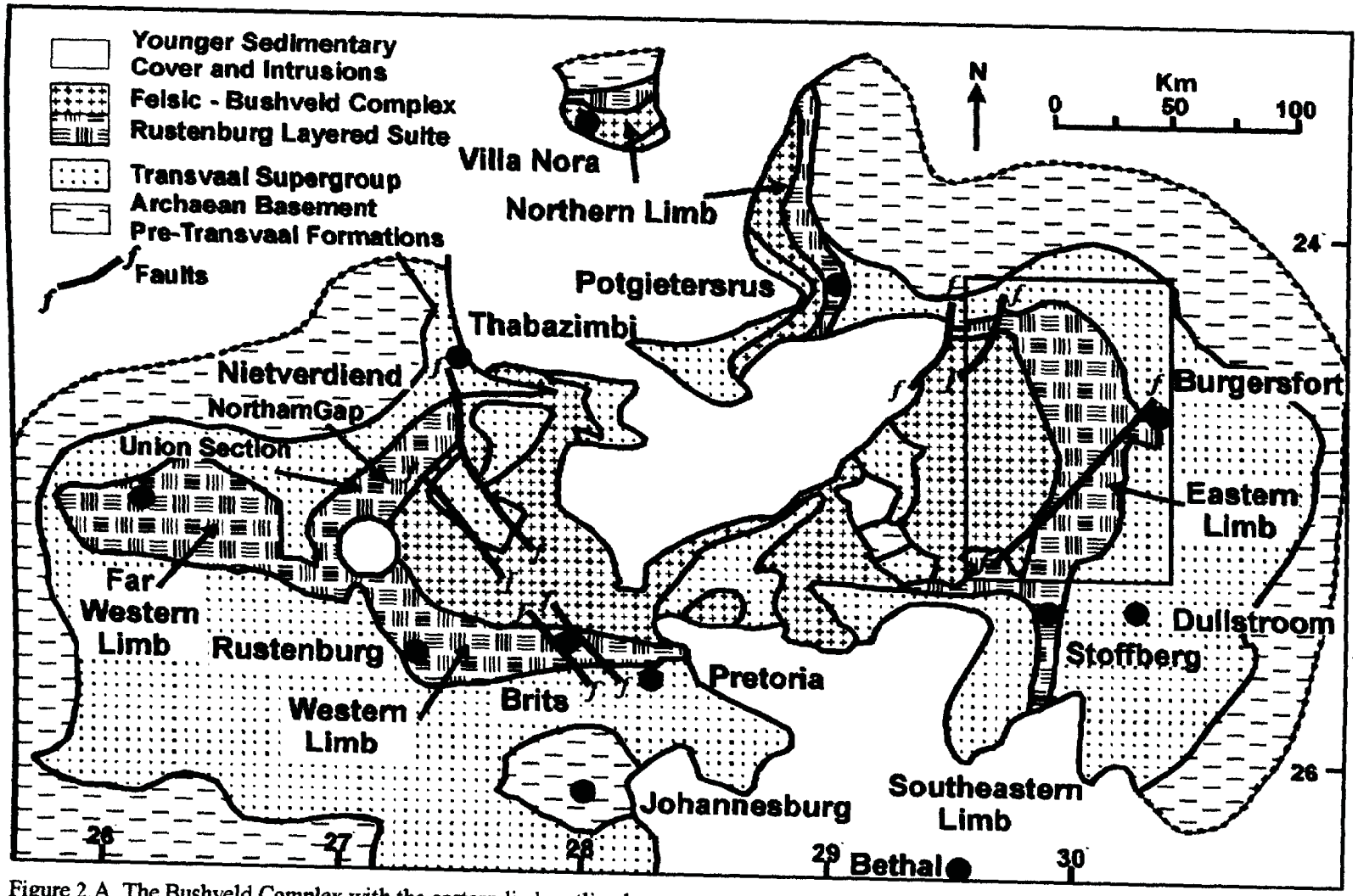


Figure 2.A The Bushveld Complex with the eastern limb outlined.

2.2: Floor Rocks and their Relationship to the Rustenburg Layered Suite

The floor rocks to the RLS in the eastern limb, between Chuniespoort and Belfast, are the Pretoria Group and the Rooiberg Group Volcanics of the Transvaal Supergroup. Seven formations within the Pretoria Group are affected by intrusion. In ascending order, these are: Silverton Shale, Magaliesberg Quartzite, Vermont Formation, Lakenvalei Quartzite, Nederhorst Formation, Steenkampsberg Quartzite and the Houtenbek Formation. The Dullstroom Basalt Formation of the Rooiberg Group Volcanics lies stratigraphically above the Pretoria Group. All are fully described by Button (1976). The degree of truncation for each formation differs for each formation, from one location to another. The Dullstroom Basalt Formation, for example, has a maximum thickness of 1400m to the west of Dullstroom, but is absent in the northern part of the limb, along with those formations down to the level of the Magaliesberg Quartzite (Button, 1976).

The dip of the floor rocks is much steeper than that of the overlying units of the Rustenberg Layered Suite, according to Button (1976), who recorded that it increases sharply from 5° to 40° approaching the contact between the mafics and the sedimentary basin. His conclusion is that, as the magmas were accommodated within the basin, further down-buckling of the floor occurred (Button, 1976). Sharp *et al.* (1981) expressed the belief that the basin had formed after the reactivation of a receding mantle-driven heat source had created a conical depression, into which magmas had migrated. Around the circumference of the complex, the lowest of the mafic units wedge out against the sedimentary basin, and the overlying upper mafic units unconformably onlap the sediments (Willemse, 1969; Button, 1976). Similarly, in the Stoffberg area, Groeneveld (1970) observed that the lower portion of the RLS has not developed from the base of the Main Zone downwards and therefore the gabbronoritic sequence of the Main Zone directly onlaps the Pretoria Group Sediments. Button (1976) suggested that some layerss, although not present at outcrop level, may occur down dip.

Immediately below the RLS, regional deformation and metamorphism of the floor rocks occurred, where temperature and pressure regimes were sufficient to increase the ductility of the sediments, causing folding. Most folds are still attached to the floor of the complex, although they are found to protrude through the cover of granites. They include the Fortdraai Anticline (Phosiri Dome), and the Schwerin, Steelpoort and Katkloof Anticlines (Sharpe and Chadwick, 1982) and are shown in Figure 2.B. The protruding nature of the floor rocks is ascribed, by Uken and Watkeys (1997), to the process of diapirism, which was initiated during the earliest magma emplacement and, they believe, to have resulted in the lateral restriction of the lowermost units of the mafic sequence.

2.3: Roof Rocks and their Relationship to the Rustenburg Layered Suite

The Rustenburg Layered Suite (RLS) intruded into the Rooiberg Group Volcanics, and transgressed the underlying sedimentary layerss of the Pretoria Group (Button, 1976; Sharpe, 1981). In the region near Sekhukhuneland, the roof sediments, which Molyneux (1974) determined were of the Pretoria Group, are sandwiched between the RLS and the overlying granophyric roof rocks. In the eastern limb, the roof rocks also include quartzite, hornfels, dolomite, leptite, and Bushveld Granites. The sediments were metamorphosed by the intruding mafics (Molyneux, 1974), and also subjected to deformation, which Button (1976) attributes to a second intrusion, that of the Bushveld Granite. Generally, the relationships within the roof rocks are poorly understood. This, Eales and Cawthorn (1996) explained, is due to the intense metamorphism and the granite emplacement. At the Malope Dome, for example, Marlow and van der Merwe (1978) describe the Bushveld Granites as apparently transgressing the rocks of the layered sequence and, consequently, the lower zones of the RLS underlie the Nebo Granite.

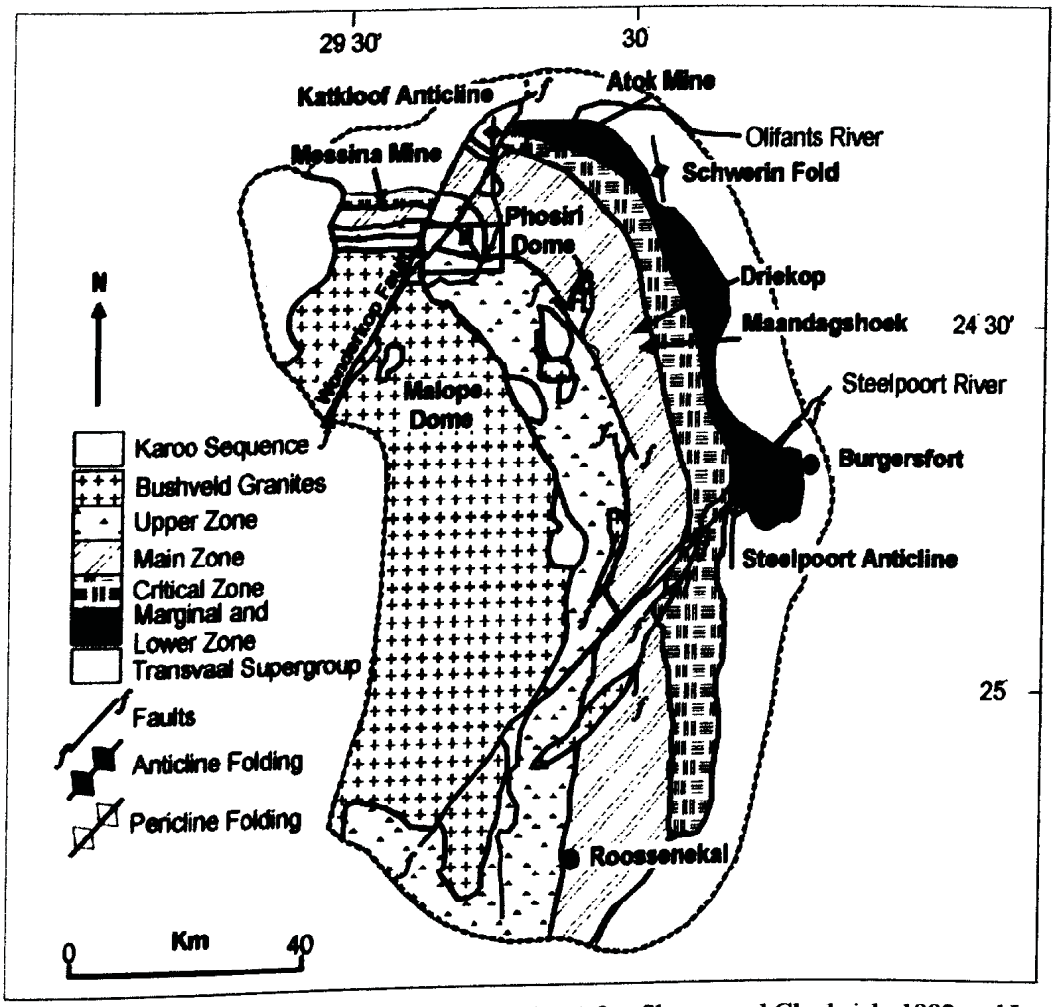


Figure 2.B The eastern limb of the Bushveld Complex (after Sharpe and Chadwick, 1982 and Lea, 1996). The southern portion of the Phosiri Dome is outlined.

2.4: Mineral Assemblage of the Rustenburg Layered Suite

The mineral assemblage in the mafic portion of the Bushveld Complex includes plagioclase, orthopyroxene, clinopyroxene and olivine, and the accessory minerals chromite, magnetite, ilmenite and apatite. Biotite, hornblende, quartz and microperthite are found by Willemse (1969) to be relatively abundant in the Upper Zone. As a result of magmatic fractionation of parent magmas, Coertze (1970) noted that differing combinations of these minerals, with their respective chemistries, form sub-unit lithologies within the individual units of the complex. Large and small scale differentiation occurs. In the case of the former, the lower sections of the RLS are chromite-rich or contain magnesium-rich olivine. Higher in the sequence, in the Upper Zone, apatite and more iron-rich magnetite are found (Coertze, 1970). Smaller scales include differentiation within the separate mineral phases, where plagioclase becomes more sodic upwards through the sequence (Coertze, 1970), olivine, forsteritic in the Lower and Critical Zones (Teigler, 1990; Eales *et al.*, 1994) which becomes more fayalitic in the Upper Zone (Molyneux, 1974). It is believed that, where there are reversals and sharp breaks in the mineral chemistry through the differentiation sequence, there was an influx of new magma into the system (Von Gruenewaldt, 1970; Kruger, 1994).

2.5: Stratigraphic Classification

The RLS has a maximum thickness of 8km (Eales and Cawthorn, 1996), which is informally subdivided into five zones and described in detail below. The Marginal Zone forms the basal unit and is followed by the Lower, the Lower and Upper Critical, the Main and the Upper Zones. Each of these is further subdivided on the basis of mineral phases either first appearing or disappearing, or by geochemical and isotopic determination of fractionation trends and reversals. There are two nomenclatures: the formal, as determined by SACS (1980); and the informal, which is more widely used and referred to in Figure 2.C.

As the mafic series of the Bushveld Complex is more exposed in outcrops in the eastern limb, much of the referenced material is derived from this area. Correlative evidence, from the western limb and other areas of the Bushveld, are mainly derived from data from underground workings and drillcores described by previous workers.

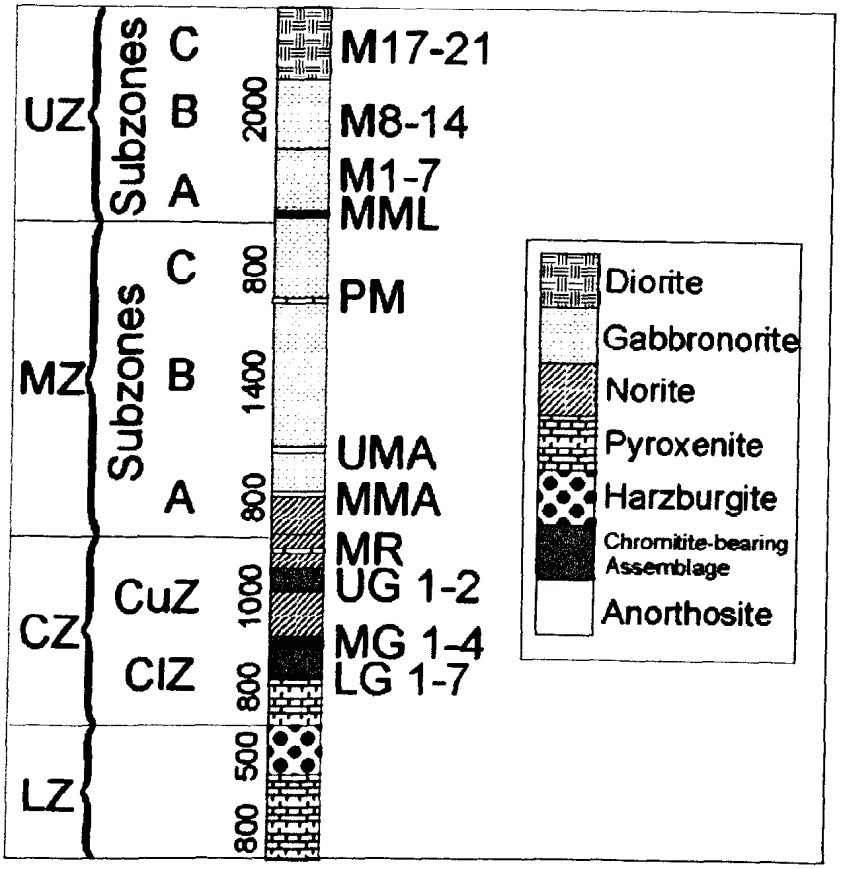


Figure 2.C Simplified stratigraphic log of the Bushveld Complex, with approximate thicknesses of zones and subzones indicated to the left of the column in meters, as found in the eastern limb. Where: UZ-Upper Zone, MZ-Main Zone, CZ-Critical Zone, CuZ-Upper Critical Zone, CLZ-Lower Critical Zone, LZ-Lower Zone, M1-21-Magnetite layers, MML-Main Magnetite Layer, PM-Pyroxenite Marker, UMA-Upper Mottled Anorthosite, MMA-Main Mottled Anorthosite, MR-Merensky Reef, UG1-2-Upper Group Chromitites, MG1-4-Middle Group Chromitites, LG1-7-Lower Group Chromitites. After Eales and Cawthorn (1996), with data from the eastern limb compiled from Von Gruenewaldt (1973), Molyneux (1974) and Cameron (1978).

2.5.1: Marginal Zone

The marginal rocks of the RLS developed between the country rocks of the Transvaal Supergroup and the layered mafic lithologies. This zone, named Shelter Norite (SACS, 1980), can be subdivided into two groups: a lower pyroxenitic and an upper gabbroic. In the eastern limb, north of Driekop, the pyroxenitic group is sandwiched between the floor sediments of the Transvaal Supergroup and the pyroxenitic units of the Lower and Critical Zones (Harmer and Sharpe, 1985). However, these same authors noted that, in the Steelpoort area, the gabbroic marginal rocks lie between the floor rocks and the Upper Critical Zone.

2.5.2: Lower Zone

The Lower Zone (LZ) comprises four separate units. In ascending order and using the SACS (1980) nomenclature these are: the Clapham Bronzitite, which is a feldspathic bronzitite; the Rostock Bronzitite, which is monomineralic; the Jagdlust Harzburgite, with olivine and bronzite; and the Serokolo Bronzitite, which is also monomineralic. However, these four units are commonly grouped together and referred to as the Lower Zone pyroxenites. Emplacement of the zone occurred at the same time as floor rock diapirism was initiated, according to Uken and Watkeys (1997). They also contend that the ponding of magma, in the depressions created by the process of dome formation, lead to the appearance of finger-like intrusions.

2.5.3: Critical Zone

The base of the Critical Zone (CZ) is defined by Cameron (1970) to be where there is an increase in interstitial plagioclase to 5%. Chromite, an important cumulus mineral also appears at the base of the CZ. The chromite is contained within the Mooihoek Pyroxenite (SACS, 1980), which essentially represents the entire Lower Critical Zone (ClZ) and includes the Lower Group (LG) Chromitites, LG1 to LG7, and two of the four Middle Group (MG) Chromitites, MG1 and MG2 (Figure 2.C). Pyroxene, olivine and chromite occur as cumulus minerals, and augite, feldspars, micas and quartz are present as a post-cumulus assemblage (Cameron, 1982). The ClZ in the westernmost sector of the eastern limb, *i.e.* the Messina Platinum Mines area, includes the LG chromitites within a lithological sequence that Lea (1996) found to be, in general, more feldspathic than he expected for this zone. He also pointed out that the top of the ClZ is marked by a disconformity at the Messina Mine and that olivine bearing lithologies are common throughout the ClZ in the central portion of the eastern limb. Gain (1985) noted that minor dunite and harzburgite occur at Maandagshoek.

The Winterveld Norite-Anorthosite first appears between MG2 and MG3 and marks the appearance of cumulus plagioclase and subsequently the base of the Upper Critical Zone (CuZ), as defined by SACS (1980). The CuZ is more laterally extensive across the eastern limb than the underlying ClZ, extending west beyond the Olifants River and south of the Steelpoort River Valley (Cameron, 1982). Apart from chromitite, the ClZ and CuZ have contrasting lithologies. SACS (1980) and Cameron (1982) attest that the CuZ is dominated by norites with minor pyroxenites, anorthosites and chromitites. The chromitite layers typically have a volume of 65% to 97% chromite, with plagioclase and orthopyroxene making up the remainder of the unit (Lee and Fesq, 1986).

This zone is also characterised by the complex cyclical layering of different lithologies, from basal chromitites and pyroxenites, through norites and leuconorites to an anorthosite capping. These cycles are not always complete and may be either gradational or abrupt at the upper and lower contacts of

each individual cycle (Eales and Cawthorn, 1996). They are also subject to lateral variation between the western and eastern limbs as described by Eales and Cawthorn (1996). In the eastern limb, for example, olivine occurs in minor proportions within the CuZ (Cameron, 1982), and is entirely absent from the Messina Mine area (Lea, 1986). Of the Upper Group Chromitites, Mossom (1986) reports that UG3 occurs only in the eastern limb, although UG1 and UG2 are present in both limbs. In the eastern limb, UG2 is contained within a pyroxenite, but varying in thickness from 360m in the north to 165m in the south (Cousins, 1969). In the western limb, this author found the same pyroxenite unit also below the Merensky Reef, varying in thickness from 12m to 24m, which is found, between 132m and 21m, below the Merensky Reef. The complete succession of the CuZ at Messina Mine occurs within a thickness of only 240 - 270m (Lea, 1996), whereas it extends to 500m thick in the Olifants River section as recorded by Cameron (1982). In the eastern limb, Cameron (1982) identified thin, coarse-grained harzburgites underlying the chromitites of the Upper Group. Harzburgites are also found further south, at the farm Maandagshoek (Gain, 1985).

In the western sector, at Messina, the footwall to the Merenksy Cyclic Unit is a succession of twelve predominantly anorthositic units with norite appearing in minor quantities (Lea, 1996). This sequence spans a vertical distance of 110m to 140m. At Maandagshoek, the UG2 - Merensky Reef interval is approximately 370m (Gain, 1985), and is described as a norite with thin layers of anorthosite and leuconorite (Cameron, 1982).

At Atok Mine, Mossom (1986) describes the footwall to the Merensky Reef, 367m above the UG3 cyclic unit, as a leuconorite containing thin layers of anorthosite and norite. The reef itself is a composite tabular unit comprising three distinct layers. From the base upwards, these are: a fine-grained poikilitic, feldspathic pyroxenite with irregular concentrations of Platinum Group Elements (PGE's), and the sulphides pentlandite and chalcopyrite, dominating pyrrhotite and pyrite; a pegmatoidal feldspathic pyroxenite; and a medium grained poikilitic, feldspathic pyroxenite, which contains the highest PGE concentration (Mossom, 1986). The middle and upper layers of the Merensky Reef are separated by two chromitite layers, approximately 50cm apart, within which lies the mineable section of the reef (Schwellnus *et al.*, 1976; Mossom, 1986). The upper pyroxenite is overlain by a norite grading into a spotted anorthosite, which is succeeded by a mottled anorthosite forming the footwall to the Bastard Reef.

As with other minerals in the CuZ, the composition of the mined reef, or potentially mineable reef, is subject to lateral variation. Mossom (1986) found that poikilitic pyroxenite occurs at Atok Mine, as opposed to pegmatoidal feldspathic pyroxenite in the Rustenburg area. Furthermore, within the Rustenburg area, the lithology hosting the mineralised reef varies from pegmatoidal pyroxenite to harzburgite and dunite (Nicholson and Mathez, 1991).

The Bastard Cyclic Unit sequence is petrologically similar to the Merensky Cyclic Unit (Mossom, 1986). However, Mossom stated that a single irregular chromitite layer is found at the base of the Bastard Reef, similar to that which is found by Lea (1986) at Messina, and little or no PGE mineralisation. The Bastard Cyclic Unit terminates at the top of the Giant Mottled Anorthosite (GMA), the uppermost unit of the CuZ (Cousins, 1969).

SACS (1980) place the upper boundary of the CZ at the top of the GMA. However, this position for the boundary placement is contested by Kruger (1990) who, on the basis of isotopic analyses, suggested that the Merensky and Bastard Cyclic Units be grouped together as "The Transitional Macro-Unit", a term first suggested for the western limb by Mitchell (1986). The outcome of Kruger's proposal would be to place the upper boundary of the CZ at an unconformity, *i.e.* the base of the Merensky Cyclic Unit.

2.5.4: Main Zone

The Main Zone (MZ) is informally divided into three separate subzones: A, B and C, with Subzone A at the base (Figure 2.C). However, the existence of Subzone C is refuted by Kruger (1990), who places the upper boundary of the MZ at the Pyroxenite Marker, which is considered to define the top of Subzone B, as described below.

Subzone A corresponds with the Winnaarshoek Norite-Anorthosite (SACS, 1980), which is 1200m thick at Sekhukhuneland (Molyneux, 1974). It is slightly thicker at 1265m in the Roossenekal area further south (Von Gruenewaldt, 1973), indicating lateral variation occurs in the eastern limb. Prominent marker layerss include the Porphyritic Norite, followed by the Main and Upper Mottled Anorthosites. The Porphyritic Norite, is recorded by Von Gruenewaldt (1973) as approximately 200m thick, and characterised by large (5mm) mottles of orthopyroxene with fine laths of included plagioclase. In the western limb, this Porphyritic Norite marks the top of the lower portion of the subzone, the lowermost 200m of which is norite alone (Mitchell, 1990). The Main Mottled Anorthosite (MMA) occurs halfway up the sequence, 565m above the base of the Main Zone, and consists of alternating layers of intermittently developed spotted and mottled anorthosites within a host of gabbronoritic rocks (Von Gruenewaldt, 1973). In the eastern limb, this layer varies in thickness from approximately 150m at Sekhukhuneland (Molyneux, 1974), to 200m in the Roossenekal area (Von Gruenewaldt, 1973). In the western limb, Mitchell (1990) also found the MMA to be 200m thick at approximately 650m above the base of the MZ. The Upper Mottled Anorthosite (UMA) measures approximately 200m thick, according to Mitchell (1990), who recorded a sequence of spotted and mottled anorthosite with gabbronorite, 950 - 1150m above the base of the MZ, similar to that found by Von Gruenewaldt (1973) and Molyneux (1974) in the eastern limb.

The first appearance of inverted pigeonite occurring alongside orthopyroxene, within a transition zone directly above the UMA and marks the base of Subzone B (Von Gruenewaldt, 1973). However, in the western limb, Wilson *et al.* (1994) measured the interval between the UMA and the first appearance of this low-calcium pyroxene as 200m in the Northern Gap area and 450m at Union Section. Above the transition zone, in the eastern limb, the orthopyroxene gives way to inverted pigeonite, which is present to the top of the subzone.

Subzone B, named the Leolo Mountain Gabbro-Norite, is characterised by a homogeneous gabbronorite that appears to have little textural variation over a total thickness of 1500m (SACS, 1980). At Roossenekal, this subzone attains a maximum thickness of 1985m, which Von Gruenewadlt (1973) ascribes to the probability of strike slip faulting. Minor anorthosite layers are developed in the Sekhukhuneland and Roossenekal areas (Molyneux, 1974; Klemm *et al.*, 1985b). Klemm *et al.* (1985a) note that cumulus magnetite appears in the stratigraphy some distance below a magnetite-rich gabbronorite, which was previously identified by Groeneveld (1970), near the top of this subzone. A pyroxenitic layer, termed the Pyroxenite Marker (Von Gruenewaldt, 1973; Molyneux, 1974) delimits the top of Subzone B. According to Klemm *et al.* (1985a), it is 2m thick in the Roossenekal area, but thins out towards the south. This layer is not only an obvious petrographical marker, but also represents a significant geochemical and isotopic break in the succession (Von Gruenewaldt, 1973; Molyneux, 1974; Sharpe, 1985; Mitchell, 1986; Kruger *et al.*, 1987; Cawthorn *et al.*, 1991). It is for these reasons that Kruger (1990) suggested that the position of the Pyroxenite Marker be the boundary between the Main and Upper Zones.

Subzone C, the Mapoch Gabbro-Norite (SACS, 1980), is 660 - 690m thick and marks the return of orthopyroxene, found alongside inverted pigeonite above the Pyroxenite Marker (Molyneux, 1974). The lithologies of Subzone C and Subzone A appear to have some similarity in that large cumulus grains of orthopyroxene exist in the lower half of Subzone C and, according to Von Gruenewaldt (1973), two mottled anorthosites occur halfway up the subzone. Above this, to the top of the MZ, the rocks appear similar to those in Subzone B, with homogenous gabbronorite and inverted pigeonite instead of orthopyroxene. In the vicinities of Stoffberg and Steelpoort respectively, Groeneveld (1970) and Molyneux (1974) determined the magnetite content to be less than 0.5%.

Centimetre-scale layering is present in the Main Zone in both eastern and western limbs (Quadling and Cawthorn, 1994; Mitchell, 1996). In the former, it occurs within a gabbronoritic unit that forms part of the footwall to the Pyroxenite Marker. A detailed study by Quadling and Cawthorn (1994) explained that, with upward progression in the sequence, the melanocratic layers become increasingly mafic, and the leucocratic layers increasingly anorthositic in nature. However, they believed that although geochemical and isotopic variation does occur in the vertical succession throughout this sequence, it is by no means systematic.

Mitchell (1990) noted cyclicity in the MZ of the western limb, but it is less pronounced than the cyclicity dominating throughout the underlying CZ. He attributed this variation to magma influxes, the frequency of which control the regularity of the cyclicity itself (Mitchell, 1990).

The boundary between the Main and Upper Zones (MZ/UZ) is defined by SACS (1980), as the interval where the first magnetite occurs within a prominent mottled anorthosite. Kruger (1990), on the other hand, suggested that the appearance of magnetite delimits a subzone boundary within the Upper Zone.

2.5.5: Upper Zone

The Upper Zone (UZ) comprises three subzones, A, B and C, which are 700m, 580m and 1000m thick, respectively (SACS, 1980), with A at the base. A further subdivision of A, into A and B, was proposed by Von Gruenewaldt (1973) and Molyneux (1974), with subsequent renaming of the second subzone to C and the third to D. This four-fold sub-division was also adopted by Klemm *et al.* (1985a), who produced a classification of the magnetite layers of the UZ, which corresponded with the four subzones. However, for the purposes of this study, the subzones are as determined by SACS (1980).

Subzone A, where magnetite first appears within a mottled anorthosite, forms the base of the UZ. Named Magnet Heights Gabbro-Norite (SACS, 1980), it includes ten separate magnetite layers. The Main Magnetite Layer (MML), situated close to the base of the subzone, is the most important economically, because of its vanadium concentration. Molyneux (1974) described a sequence from the base of Subzone A, where inverted pigeonite is present to the top of the mafic layered sequence, in the Sekhukhuneland area. The only exception to this is within a pyroxenite, where orthopyroxene is the only low-Ca pyroxene, that is situated above the MML. These observations are similar to those made by Von Gruenewaldt (1973).

Subzone B, known as the Ironstone Magnetite Gabbro (SACS, 1980), begins where a cumulus iron-rich olivine appears. Overlying a sequence of olivine gabbro is a 500m thick magnetite-rich gabbro, which hosts seven thin magnetite layers (SACS, 1980).

Subzone C, named the Luipershoek Olivine Diorite (SACS, 1980), is denoted by three unique features: the appearance of small cumulus apatite crystals, which constitute 5% of the lithology; a major cumulus phase of iron-rich olivine, which is an important mineral for the majority of the unit; and the composition of cumulus plagioclase changes from labradorite to andesine (SACS, 1980). A further seven magnetite layers are hosted within this subzone, according to Von Gruenewaldt (1973).

Olivine may be absent from the Subzones B and C, as Buchanan (1975) discovered in the Bethal area of the eastern limb, where he also noticed that the Main and Critical Zones were missing. Buchanan (1975) offered two explanations for the absence of these two zones. Either the magma, which had crystallised in the Bethal area, migrated to this location at a relatively late stage of its fractionation. Or the magma, from which these lithologies formed, represents a separate pipe from that which feeds into the remainder of the Bushveld Complex.

2.6: Magmatic Influxes

Several magmatic influx events are considered to have taken place and are summarised by Sharpe (1981). Proceeding upwards, from the bottom of the mafic sequence, the sites of the three major magma additions are: the base of the LZ, the level of the Merensky Reef, and the Pyroxenite Marker, where the final episode occurred. Hatton and Von Gruenewaldt (1990) suggested that another influx of magma, which was plagioclase saturated, occurred between the ClZ and CuZ. The sequence above the Pyroxenite Marker to the top of the UZ differentiated, without further interruption, to the top of the Upper Zone (Molyneux, 1974; Kruger *et al.*, 1987). From an evaluation of the cooling and crystallisation trends of the Bushveld Complex, Cawthorn and Walraven (1997) defined a model, which implies that a lateral expulsion of magma, from a previous influx, occurred at the Pyroxenite Marker, at the same time as a new injection of magma. They calculate that at the rate of emplacement was $6km^3$ per year, for the entire 8km thick complex, which crystallised during a 150 000 year period.

2.7: Connectivity of the Eastern and Western Limbs

Cawthorn *et al.* (1998) summarise several important factors that lead to the interpretation that the eastern and western limbs of the Bushveld Complex are connected at depth. They claim that, although differentiation can produce similar trends from similar magmas that are not connected, reversals may not necessarily occur at the same horizons. The presence of such reversals and breaks in the geochemical trends, and the initial strontium ratios that are found on both eastern and western limbs, is evidence that points to a connection between the limbs. Cawthorn *et al.* (1998) cite further evidence to support this belief. Common to both limbs are: cumulus phases appear at similar horizons e.g. plagioclase at the top of the MG2; bifurcating anorthosite lenses within the footwall chromitite stringers of the UG1; and similar grades of PGE's in the UG2.

In 1959, Cousins used gravity profiles of the Bushveld Complex to claim that the eastern and western limbs were not connected at depth. However, based on updated gravity profiles, Meyer and de Beer (1987) argued that there is a reduced gravity anomaly in the centre of the complex. A more recent interpretation, by Cawthorn *et al.* (1998), implies that the Bushveld Complex was large enough to

depress the underlying crust by up to 5km into the mantle, in the central region by the Bushveld magma. Isostatic rebound of the crust has since caused the displacement of this gravity anomaly. Their model illustrates how the gravity anomaly, for the centre of the complex, could be brought into line with the profiles of the eastern and western limbs, and therefore account for the observed present day anomaly (Cawthorn *et al.*, 1998).